

# Improved photocatalytic activity by utilizing the internal electric field of polar semiconductors: a case study of self-assembled NaNbO<sub>3</sub> oriented nanostructures†

Cite this: *RSC Adv.*, 2014, 4, 3165

Linqin Jiang,<sup>a</sup> Yaohong Zhang,<sup>a</sup> Yu Qiu<sup>b</sup> and Zhiguo Yi<sup>\*a</sup>

How to promote separation of photo-generated carriers is one of the key issues determining the photocatalytic activity of a semiconductor. In this paper, we report a new strategy that utilizing an internal electric field of polar semiconductors to improve photocatalytic activity and, proving it by liquid-phase photodegradation (photocatalytic RhB degradation) as well as gas-phase photodegradation (photocatalytic oxidation of CH<sub>4</sub>) experiments upon the self-assembled NaNbO<sub>3</sub> oriented nanocuboids that were fabricated by a facial hydrothermal route. The formation conditions and mechanisms of the ordered nanostructures were also discussed.

Received 20th October 2013  
Accepted 30th October 2013

DOI: 10.1039/c3ra45954c

www.rsc.org/advances

## 1 Introduction

Semiconductor photocatalysis has attracted extensive and increasing attention due to its applications in environmental cleansing as well as solar fuel production.<sup>1</sup> Its basic principle involves photogenerated electrons and holes migrating to the surface of the semiconductor and serving as redox sources which then react with adsorbed chemicals, leading to the redox reactions.<sup>1d</sup> Light absorption, redox potentials and the recombination of photogenerated carriers are amongst the key factors determining the photocatalytic activities. Intensive research on the development of high activity photocatalysts in the past several decades has witnessed great success with strategies such as new material exploration,<sup>2</sup> band engineering,<sup>3</sup> co-catalysts loading,<sup>4</sup> crystal facet engineering,<sup>5</sup> photoelectrode design,<sup>6</sup> *etc.* Nevertheless, how to promote spatial separation of photo-generated electrons and holes within a photocatalyst interior remains a challenge.

Fabrication of a junction structure is an effective approach for the promotion of charge separation.<sup>7</sup> Co-catalysts loading has the same effect besides their function of reducing the overpotential of chemical reactions.<sup>4</sup> However, these only function at the interfaces. Herein, we report improving the

photocatalytic activity by utilizing the internal electric field of polar semiconductors with a case study of self-assembled NaNbO<sub>3</sub> oriented nanostructures.

A polar semiconductor has spontaneous electric polarization showing important applications in electronic information technology.<sup>8</sup> Early research on new catalyst exploration has shown that a lot of polar semiconductors are good photocatalysts, for example, CdS,<sup>9</sup> WO<sub>3</sub>,<sup>10</sup> SrTiO<sub>3</sub>,<sup>11</sup> Bi<sub>2</sub>WO<sub>6</sub>,<sup>12</sup> (K, Na) TaO<sub>3</sub>,<sup>13</sup> *etc.* It is obvious that electric polarization helps the separation of electrons and holes (Fig. 1a and b). However, since it is relatively difficult to control the polarization states of powder samples (Fig. 1c), there are fewer reports on conscious application of the effect of electric polarization to powder photocatalysis.<sup>14</sup> Current research is based on the consideration that spontaneous electric polarization of a polar semiconductor can be utilized to realize the spatial separation of photogenerated electrons and holes within the interior of a semiconductor photocatalyst if the semiconductor micro/nano-crystals can be fabricated and their assemblage state can be well controlled. The possible patterns satisfying this point of view are schematically shown in Fig. 1d and e.

## 2 Experimental

### 2.1 Preparation of photocatalysts

The NaNbO<sub>3</sub> samples were prepared by hydrothermal synthesis. All reagents were analytically pure, commercially available and used without further purification. In a typical procedure, 0.01 mol of Nb<sub>2</sub>O<sub>5</sub> (4 N, Sinopharm Chemical Reagent Co. Ltd) and 1 M of NaOH (AR, 96% min, Sinopharm Chemical Reagent Co. Ltd) were dissolved in 70 ml deionized H<sub>2</sub>O. After 1 h of magnetic stirring, the precursor solution was transferred into

<sup>a</sup>Key Laboratory of Optoelectronic Materials Chemistry and Physics, Fujian Institute of Research on the Structure of Matter, Chinese Academy of Sciences, Fuzhou 350002, China. E-mail: zhiguo@fjirsm.ac.cn

<sup>b</sup>New Energy Technology Center, Shanghai Institute of Microsystems and Information Technology, Chinese Academy of Sciences, Shanghai 201807, China

† Electronic supplementary information (ESI) available: UV-vis spectral changes of RhB, degradation kinetics, FTIR spectra, CH<sub>4</sub> conversion, SEM images of thin films, XRD patterns, and SEM images of NaNbO<sub>3</sub> nanostructures, *etc.* See DOI: 10.1039/c3ra45954c

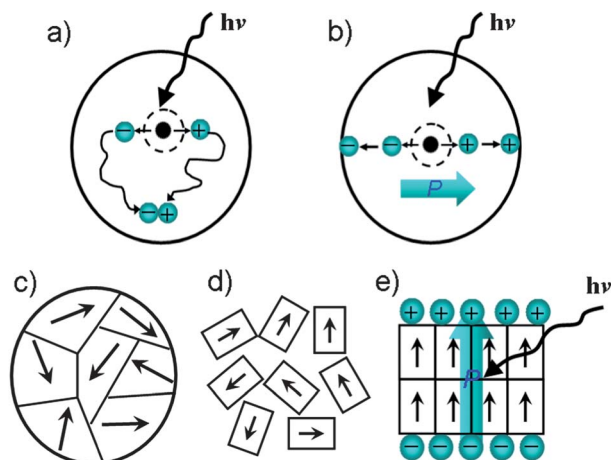


Fig. 1 Diagram showing: (a) recombination of photo-generated electrons and holes within a photocatalyst interior; (b) separation and transportation of photo-generated electrons and holes driven by the electric field of spontaneous polarization  $P$  in the interior of a polar semiconductor; (c) powder sample with disordered distribution of  $P$ ; (d) monodisperse single crystal particles with  $P$ ; (e) powder sample with ordered arrangement of single crystal particles. For simplicity, the case of a single crystal with multi-domain states was omitted in the diagram.

a Teflon-lined steel autoclave. The autoclave was sealed, heated at 200 °C for 24 h and then cooled down to room temperature naturally. The final product was washed with deionized water and pure alcohol several times to remove the residues, and then dried at 80 °C overnight. The samples obtained in the presence of 1, 2.5, 5 and 8 M of NaOH were denoted as NNB-1, NNB-2, NNB-5 and NNB-8, respectively. Other samples were synthesized by changing the concentration of NaOH as well as the dwelling time.

## 2.2 Cocatalyst loading

For cocatalyst loading,  $\text{H}_2\text{PtCl}_6 \cdot 6\text{H}_2\text{O}$  (AR, Sinopharm Chemical Reagent Co. Ltd) was used as a Pt precursor. 1.0 wt% of Pt was loaded on the  $\text{NaNbO}_3$  samples by an impregnation method or by a photodeposition method. In the impregnation method, the photocatalyst (0.2 g) was dispersed into an aqueous methanol solution (30 ml) of the metal precursor for 1 h, followed by evaporation to dryness overnight. Then, the dried powder was calcined in air atmosphere at 400 °C for 2 h. In the photodeposition method, the photocatalyst was dispersed in methanol solution with vigorous stirring, followed by photoirradiation from the above using a 300 W Xe lamp, which was entirely emitted from UV to visible light, for 2 h, with continuous stirring. The NNB-1 (or NNB-8) samples with the Pt cocatalyst by the impregnation method and by photodeposition were referred to as Pt–NNB-1 (or Pt–NNB-8) and Pt–NNB-1-LD (or Pt–NNB-8-LD), respectively.

## 2.3 Physical characterization

Phase identification of the samples was determined by X-ray diffraction (XRD, Rigaku Miniflex II). The size and morphology

of the samples were examined by scanning electron microscopy (SEM, JSM-6700F), transmission electron microscopy (TEM), high-resolution TEM (HRTEM) and electron diffraction (ED) pattern were taken on JEM-2010. UV-vis diffuse reflectance spectra of the samples were recorded on a PerkinElmer Lambda 950 UV/vis/NIR spectrometer. The surface area of the samples was measured by Brunauer–Emmett–Teller (BET, ASAP 2020C + M). FTIR measurements were carried out by a FT-IR spectrometer (Spectrum one, PerkinElmer).

## 2.4 Photodegradation of RhB

The photocatalytic activity experiments of the samples for degradation of RhB were performed under ice–water bath conditions with a 300 W Xe arc lamp as the light source. Typically, 30 mg NNB-1 powder was mixed with RhB (2 ml, with a concentration of 40  $\text{mg L}^{-1}$ ) in a 198 ml  $\text{H}_2\text{O}$  solution. The suspension was magnetically stirred for 1 h to reach complete adsorption–desorption equilibrium in the dark and subsequently exposed to sunlight simulator irradiation with maximum illumination time up to 240 min. The excitation source is located at *ca.* 12.2 cm away from the suspension surface. During the irradiation, the suspension was continuously stirred and the reaction system was kept in an ice–water bath. Before irradiation and at certain time intervals, about 7 ml suspensions were sampled and centrifuged three times to remove the residuals before characterization. The concentration of RhB was determined by measuring the absorbance in step time using UV-vis-NR spectrophotometers (Lambda-900, PerkinElmer).

## 2.5 Photooxidation of $\text{CH}_4$

Photocatalytic oxidation of  $\text{CH}_4$  was examined upon  $\text{NaNbO}_3$  or Pt-loaded  $\text{NaNbO}_3$  samples in a fixed-bed photoreactor. The catalyst (0.15 g) was spread on the flat bottom of the reactor (450 ml). The reaction gas, a mixture of  $\text{CH}_4$  (0.5 ml) and  $\text{O}_2$  (5 ml), was introduced into the reactor after removing the air in the cell by  $\text{N}_2$  carrier for 20 min. The reaction was carried out without heating at atmospheric pressure upon photoirradiation from a 300 W xenon lamp located at *ca.* 15 cm away from the catalyst surface. At certain time intervals, the products in the gaseous phase were sampled and analyzed by gas chromatography (Fuli Instrument GC9720, China).

## 2.6 Photoelectrochemical measurement

The fluorine doped tin oxide (FTO) substrates were cleaned by ultrasonication in distilled water and absolute ethanol for 30 min sequentially. One edge of the conducting glass substrates was covered with adhesive tape. Typically, the suspension was prepared by grinding 0.5 g of  $\text{NaNbO}_3$  powder, 2.5 g of ethyl cellulose (10%) ethanol solution and 1.75 g terpineol. Then the homogeneous slurries were spread on a FTO glass substrate by the spin-coating method. The film was dried in air and annealed at 550 °C for 15 min. The photocurrent was measured by an electrochemical analyzer (CHI660D Instrument) in a standard three-electrode system with  $\text{NaNbO}_3$  film as the working electrode, Pt wire as the counter electrode, and

Ag/AgCl electrode as a reference electrode. A 500 W Xe arc lamp was utilized as the light source. A 0.5 M Na<sub>2</sub>SO<sub>4</sub> aqueous solution was used as the electrolyte.

### 3 Results and discussion

In light of our previous experience on polar oxides,<sup>15</sup> NaNbO<sub>3</sub> semiconductor was taken as a research sample and was fabricated *via* a hydrothermal route to corroborate the above point of view. Scanning electron microscopy (SEM) images (Fig. 2a–c) of the fabricated samples exhibit assemblages of nanocuboids with side lengths varying from hundreds of nanometers to several micrometers and by way of contrast, with increasing the NaOH concentration of NaNbO<sub>3</sub> nanocuboids assembled from ordered *b*-axis orientation (Fig. 2a and b) to disordered random distribution (Fig. 2c). X-Ray diffraction (XRD) patterns of the synthesized samples were all identified to be a typical orthorhombic NaNbO<sub>3</sub> structure type (JCPDS 33-1270) with well developed crystallinity. No extra peaks except for the orthorhombic NaNbO<sub>3</sub> phase were detected from the XRD analysis. Fig. 2d shows XRD patterns of two typical samples (NNB-1 and NNB-8) with ordered and disordered arrangement of NaNbO<sub>3</sub> particles, respectively. The fabrication conditions as well as the basic physical parameters of the two samples are listed in Table 1.

Transmission electron microscopy (TEM) analysis of an individual NaNbO<sub>3</sub> particle further confirms its cuboid-shaped structure with unequal side lengths of *a*–*c* plane (Fig. 3a). High-resolution TEM (HRTEM) (Fig. 3b) reveals the highly crystalline characteristics of the nanocuboid. The sharp lattice fringes with an interplanar lattice spacing of 0.391 nm correspond to the (101) atomic plane. The corresponding selected-area electron diffraction (SAED) pattern (Fig. 3c and S1†) indicates a single-crystalline feature of the nanocuboid. Note the weak satellite

diffraction spots and streakings observed in the SAED pattern are correlated with the distortion of NbO<sub>6</sub> octahedra and atomic displacement in the polar NaNbO<sub>3</sub> structure (Fig. 3d), respectively.<sup>16</sup> Further details of this kind of superstructures can be found in ref. 15a and b.

It is known the NaNbO<sub>3</sub> crystal is antiferroelectric along the *c* axis and ferroelectric along the *b* axis.<sup>16</sup> This means there is an internal bias electric field along the *b* axis and when the single crystal nanocuboids assemble into oriented nanostructures the internal bias electric field can yield the greatest returns on the separation as well as transportation of photon-generated carriers (as shown in Fig. 1e). Instead, when the single crystal nanocuboids assemble into disordered nanostructures the randomly distributed internal bias electric field within individual nanocuboids will make less electrons and holes move to the surface of the samples (as shown in Fig. 1c). Therefore, the ordered and disordered NaNbO<sub>3</sub> nanostructures fulfill the cases described in Fig. 1e and c respectively. Two photocatalytic experiments were then carried out to examine the activity of the samples.

The first one is Rhodamine B (RhB) photodegradation in aqueous solution. The NaNbO<sub>3</sub> samples involved include the ordered NNB-1, disordered NNB-8, and the disordered NNB-1 after mechanical milling. From the temporal evolution of the spectral changes (Fig. S2†), it is found that the adsorption effects of the samples are negligible. The decrease in absorption intensity as well as its wavelength shift suggest the de-ethylation reaction and cleavage of the RhB chromophore ring structure<sup>17</sup> occurred simultaneously during the photocatalytic experiments. Using the major absorption band at about 554 nm to determine the concentration of RhB, we can compare the photocatalytic activities of the ordered and disordered NaNbO<sub>3</sub> samples, as shown in Fig. 4a. The disordered samples show obviously weaker activities. For instance, after 3 h illumination under simulated sunlight the photodegradation efficiency of RhB upon the ordered NNB-1 and disordered NNB-8 reaches 100% and *ca.* 60%, respectively. Further investigation of reaction kinetics indicates that the ordered NNB-1 exhibits a much higher apparent reaction rate constant ( $k = 0.0249 \text{ min}^{-1}$ ) than the disordered NNB-8 ( $k = 0.00444 \text{ min}^{-1}$ ) (Fig. S3†). FTIR results (Fig. S4†) reveal further the destruction of RhB chromophore ring structure occurred more deeply upon the ordered NaNbO<sub>3</sub> sample than that upon the disordered ones since the peak attributed to the characteristic vibration of the aromatic ring structure<sup>18</sup> became much weaker after illumination upon the ordered NaNbO<sub>3</sub> sample.

In view of the fact that RhB can also harvest sunlight, experiments with RhB photodegradation upon the ordered NNB-1 and disordered NNB-8 under modified illumination conditions were designed to test the possibly evolved effects of photosensitization. From UV-vis absorption spectra (Fig. S2†), it is clear that RhB can be excited by visible light whereas the NaNbO<sub>3</sub> samples can be excited only by a wavelength shorter than ~380 nm (Fig. 4b). Therefore, we used a cut filter of 420 nm to excite the RhB but prevent the excitation of the NaNbO<sub>3</sub> samples. It was found that the RhB degradation upon the disordered NNB-8 was governed by the

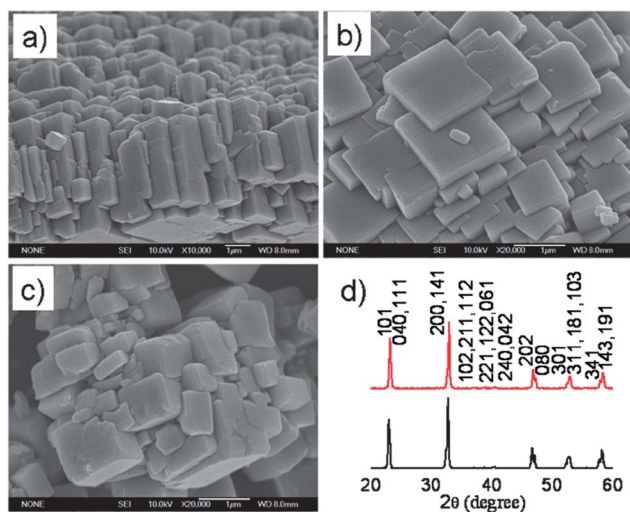


Fig. 2 (a–c) SEM images of: (a) and (b) NaNbO<sub>3</sub> samples with ordered nanocuboid assemblage taken from different directions; (c) the NaNbO<sub>3</sub> samples with disordered nanocuboid assemblage; (d) XRD patterns of the ordered and disordered NaNbO<sub>3</sub> samples prepared at [NaOH] = 1 M (upper one) and at [NaOH] = 8 M (lower one).

Table 1 Fabrication conditions as well as some basic physical parameters of two typical NaNbO<sub>3</sub> samples

Sample	Synthesis conditions	Lattice parameters	Band gap (eV)	BET surface (m <sup>2</sup> g <sup>-1</sup> )
NNB-1 (ordered)	[NaOH] = 1 M, 200 °C, 24 h	$a = 5.473 \text{ \AA}$ $b = 15.553 \text{ \AA}$ $c = 5.537 \text{ \AA}$	3.26	1.313
NNB-8 (disordered)	[NaOH] = 8 M, 200 °C, 24 h	$a = 5.535 \text{ \AA}$ $b = 15.527 \text{ \AA}$ $c = 5.508 \text{ \AA}$	3.26	4.488

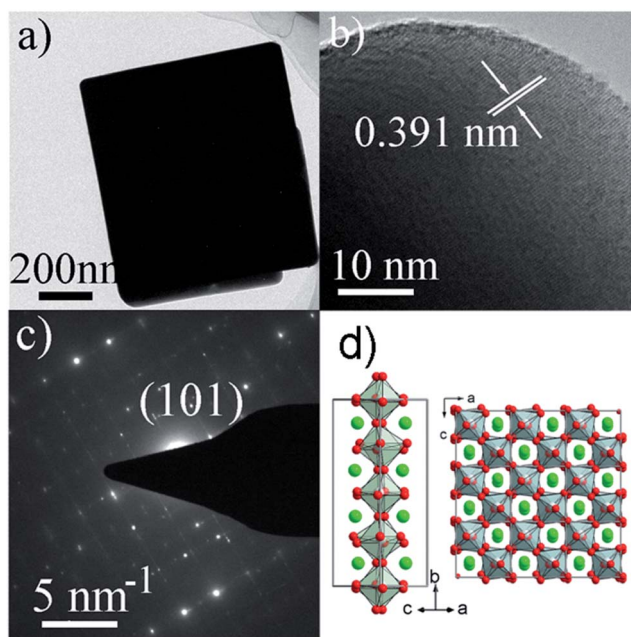


Fig. 3 (a) TEM image, (b) HRTEM image, (c) ED pattern of a NaNbO<sub>3</sub> nanocuboid (NNB-1 sample); (d) crystal structure of NaNbO<sub>3</sub> where Na ions are located in the cavities of NbO<sub>6</sub> octahedra. Note the material is ferroelectric along the *b* axis.<sup>16</sup>

indirect photosensitization and the high RhB degradation activity upon the ordered NNB-1 (Fig. 4a) is largely determined by the intrinsic excitation of the NaNbO<sub>3</sub> semiconductor. From the peak profiles of XRD patterns (Fig. 2d) we know both the NNB samples exhibit well developed crystallinity. The BET surface area measurements indicate that BET surface area of the NNB-8 (4.488 m<sup>2</sup> g<sup>-1</sup>) is larger than that of the NNB-1 (1.313 m<sup>2</sup> g<sup>-1</sup>). From these facts we can conclude that the state of assemblage of the nanocuboids accounts for the differences of photocatalytic activity between the NaNbO<sub>3</sub> samples. The stability of the NNB-1 during photocatalytic reaction was further explored by recycling tests (Fig. S5†). The photocatalytic activity of the ordered NaNbO<sub>3</sub> nanocuboids decreases to some extent during the second cycle, indicating the ordered nanostructure of the NNB-1 sample will be destroyed after long time stirring.

The second photocatalytic experiment is photocatalytic oxidation of methane (CH<sub>4</sub> + O<sub>2</sub> → CO<sub>2</sub> + H<sub>2</sub>O). The photocatalytic activities of the NaNbO<sub>3</sub> samples were compared in Fig. 4c (as well as shown in Fig. S6† the conversion of methane).

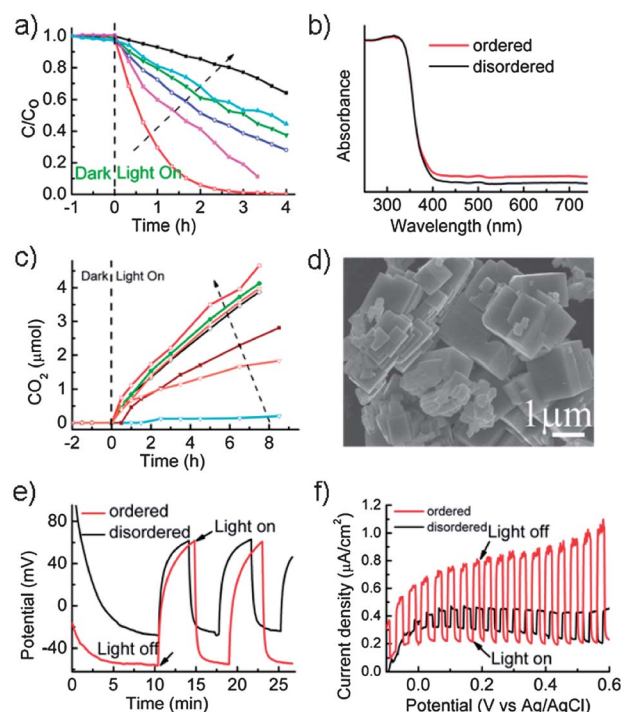


Fig. 4 (a) Photodegradation of RhB upon the samples (along the direction of the arrow with broken line): the ordered NNB-1 under sunlight, the disordered NNB-1 after mechanical milling under sunlight, the ordered NNB-1 under visible light, the disordered NNB-8 under sunlight, the disordered NNB-8 under visible light, and without catalyst under sunlight; (b) UV-vis diffuse reflectance spectra of the ordered NNB-1 and disordered NNB-8 samples; (c) CO<sub>2</sub> generation from CH<sub>4</sub> photo-oxidation upon the samples (along the direction of the arrow with broken line): without catalyst, Pt-NNB-1, Pt-NNB-1-LD, NNB-8, Pt-NNB-8, Pt-NNB-8-LD, and NNB-1, under the same sunlight illumination respectively; (d) SEM image of Pt-NNB-1 sample prepared by the impregnation method. (e) Open circuit photovoltage curves; (f) current-potential curves of thin films prepared by ordered NNB-1 and disordered NNB-8 respectively.

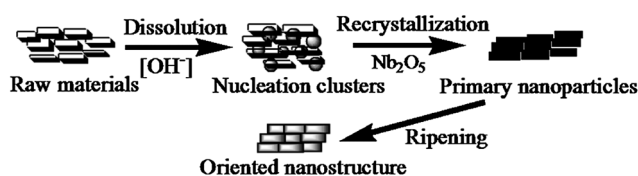


Fig. 5 Schematic illustration of the growth mechanism of the ordered NaNbO<sub>3</sub> nanostructure.

Obviously, the CO<sub>2</sub> production rate upon the ordered NNB-1 is higher than that upon the disordered NNB-8. The effect of cocatalyst loading was investigated as well. Herein 1 wt% Pt was loaded by an impregnation method on NNB-1 (named as Pt–NNB-1) and NNB-8 (named as Pt–NNB-8), respectively. For comparison purposes, the same amount of Pt was also loaded by a photodeposition method on NNB-1 (named as Pt–NNB-1-LD) and NNB-8 (named as Pt–NNB-8-LD), respectively. Both the samples prepared by the photodeposition method exhibit higher activity than their counterpart prepared by the impregnation method. In addition, regardless of the loading method the Pt-loaded NNB-8 shows higher activity than the NNB-8. However, it is interesting to note that both the Pt-loaded NNB-1 samples exhibit much lower activity than the NNB-1 sample in gas phase photocatalysis, although the Pt–NNB-1 sample shows significantly higher activity on RhB degradation than the NNB-1 in aqueous environment (Fig. S7†). SEM observations of the Pt loaded NNB-1 samples indicate that the ordered nanostructure of NNB-1 was destroyed during the process of Pt loading, as shown in Fig. 4d. Thus it can be concluded that keeping the ordered NaNbO<sub>3</sub> nanostructure intact is important for the improvement of CH<sub>4</sub> oxidation.

The results of the above two experiments undoubtedly corroborate our point of view that the internal electric field of a polar semiconductor can be utilized to improve photocatalytic activity if the semiconductor particles and polarization direction are carefully controlled. Moreover, based on the description in Fig. 1 one can infer that (I) there is (photo)voltage between the two end surfaces along the *b* axis of a NaNbO<sub>3</sub> nanocuboid and (II) photocurrent in the ordered NaNbO<sub>3</sub> nanostructure should be larger than that in the disordered NaNbO<sub>3</sub> nanostructure.

To examine this deduction we fabricated thin film samples using the ordered and disordered nanostructures respectively and measured their photoelectrochemical responses. SEM observations indicate that the orientation characteristic of the ordered nanostructure was partially retained (Fig. S8†). The evidently larger open-circuit photovoltage (Fig. 4e) as well as larger photocurrent density (Fig. 4f) of the ordered NaNbO<sub>3</sub> thin film certainly support the aforementioned inference.

During the hydrothermal synthesis we did not obtain mono dispersed NaNbO<sub>3</sub> (nano)crystals except for the assemblages of oriented NaNbO<sub>3</sub> nanocuboids. The only reactants used in the hydrothermal synthesis were pure Nb<sub>2</sub>O<sub>5</sub> and NaOH. How the orientated NaNbO<sub>3</sub> nanostructures generated? To understand this, a series of synthesis experiments were carried out where we adjusted either NaOH concentration or dwelling time.

The relationship between the NaOH concentration and the microstructure of NaNbO<sub>3</sub> was established by fixing the reaction temperature (200 °C) as well as dwelling time (24 h), as shown in Fig. S9 and S10.† When setting the concentration of NaOH from 1 M to 8 M, all the prepared samples were identified by XRD to be pure phase of NaNbO<sub>3</sub>. However, the morphologies of the samples prepared under different NaOH concentration were observed to be different as shown in Fig. S10.† When increasing the NaOH concentration to 8 M, the ordered nanostructures were destroyed completely. Therefore, it is suggested that the

ordered NaNbO<sub>3</sub> “cuboid-by-cuboid” arrays can only be obtained under low NaOH concentration (*e.g.* 1 M) under fixed dwelling time. Increasing the NaOH concentration (*e.g.* 8 M) will destroy the ordered nanostructures.

The influence of dwelling time was performed by fixing the NaOH concentration (1 M) and reaction temperature (200 °C) (Fig. S11–S12†). The pure phase NaNbO<sub>3</sub> was obtained after 6 h reaction, as seen in Fig. S11.† The XRD patterns of the as-prepared sample for 0–3 h actually reflect the chemical of Nb<sub>2</sub>O<sub>5</sub>. With increasing the dwelling time, the peaks attributed to Nb<sub>2</sub>O<sub>5</sub> disappear gradually and the new peaks attributed to NaNbO<sub>3</sub> emerge, which suggest that the process of dissolution–recrystallization happens for the preparation of orthorhombic NaNbO<sub>3</sub>. The SEM images in Fig. S12† further reveal that there are two processes occurred simultaneously during the hydrothermal processing. One is recrystallization of the dissolved Nb<sub>2</sub>O<sub>5</sub> on the surface of the undissolved Nb<sub>2</sub>O<sub>5</sub> to form orientated structures. The other is the generation of NaNbO<sub>3</sub> nanoparticles on the surface of the orientated structures of Nb<sub>2</sub>O<sub>5</sub>. The Nb<sub>2</sub>O<sub>5</sub> assemblage at the initial stage of hydrothermal synthesis acts as a template inducing the growth of self-assembled NaNbO<sub>3</sub> ordered nanostructure. The growth process of ordered nanostructure is therefore schematically shown in Fig. 5 and explained as follows:

During the hydrothermal treatment, the superficial part of Nb<sub>2</sub>O<sub>5</sub> particles first hydroxylize and dissolve into the solution with the aid of OH<sup>−</sup>.<sup>19</sup> At low NaOH concentration (*e.g.* 1 M), the alkalinity is too low to dissolve the whole Nb<sub>2</sub>O<sub>5</sub> powder. Under such a condition, two processes occur simultaneously. One is recrystallization of the dissolved Nb<sub>2</sub>O<sub>5</sub> on the surface of the undissolved Nb<sub>2</sub>O<sub>5</sub> to form orientated structures. The other is the generation of NaNbO<sub>3</sub> nanoparticles on the surface of the orientated structures of Nb<sub>2</sub>O<sub>5</sub>. The Nb<sub>2</sub>O<sub>5</sub> orientated structure acts as a sacrificial template in the subsequent stages. With prolonging the dwelling time, the ordered NaNbO<sub>3</sub> “cuboid-by-cuboid” arrangement generates gradually under the process of nucleation and Ostwald ripening. Raising NaOH concentration tends to increase the solubility of Nb<sub>2</sub>O<sub>5</sub>. At high NaOH concentration (*e.g.* 8 M), the Nb<sub>2</sub>O<sub>5</sub> is dissolved completely and can not form orientated template in the following stages. Under such a condition, what's obtained finally is NaNbO<sub>3</sub> nanocuboids with disordered assemblage.

## 4 Conclusions

In summary, we have suggested a strategy that utilizing internal electric field of polar semiconductors to improve photocatalytic activity and, the strategy is evidenced by both photocatalytic RhB degradation and CH<sub>4</sub> oxidation upon the self-assembled NaNbO<sub>3</sub> oriented nanocuboids that fabricated by a facial hydrothermal route. Given the resulting self-assembled NaNbO<sub>3</sub> oriented nanostructure as well as the strategy corroborated, it is expected that the present results would trigger further interest not only in the fabrication of complex nanostructures with controllable crystalline morphology, orientation and surface architectures but also in the application of polar semiconductors in solar energy utilization.

## Acknowledgements

This work was financially supported by the National Key Project on Basic Research (Grant no. 2013CB933203), the Natural Science Foundation of China (Grant no. 21373224), the Natural Science Foundation of Fujian Province (Grant no. 2012J01242), and the One Hundred Talent Program of the Chinese Academy of Sciences.

## References

- (a) T. Leshuk, R. Parviz, P. Everett, H. Krishnakumar, R. A. Varin and F. Gu, *ACS Appl. Mater. Interfaces*, 2013, **5**, 1892–1895; (b) H. U. Lee, S. C. Lee, S. H. Choi, B. Son, S. J. Lee, H. J. Kim and J. Lee, *Appl. Catal., B*, 2013, **129**, 106–113; (c) G. S. Pozan, M. Isleyen and S. Gokcen, *Appl. Catal., B*, 2013, **140–141**, 537; (d) A. L. Linsebigler, G. Q. Lu and J. T. Jr Yates, *Chem. Rev.*, 1995, **95**, 735–758; (e) A. J. Bard and M. A. Fox, *Acc. Chem. Res.*, 1995, **28**, 141–145; (f) N. S. Lewis and D. G. Nocera, *Proc. Natl. Acad. Sci. U. S. A.*, 2006, **103**, 15729–15737; (g) X. Chen, S. Shen, L. Guo and S. S. Mao, *Chem. Rev.*, 2010, **110**, 6503–6570.
- (a) P. Basnet, G. K. Larsen, R. P. Jadeja, Y.-C. Hung and Y. Zhao, *ACS Appl. Mater. Interfaces*, 2013, **5**, 2085–2095; (b) Y. C. Zhang, M. Yang, G. Zhang and D. D. Dionysiou, *Appl. Catal., B*, 2013, **142–143**, 249–258; (c) Y. C. Zhang, L. Yao, G. Zhang, D. D. Dionysiou, J. Li and X. Du, *Appl. Catal., B*, 2014, **144**, 730–738; (d) H. Y. Kang and H. P. Wang, *Environ. Sci. Technol.*, 2013, **47**, 7380–7387; (e) W. Wang, J. C. Yu, D. Xia, P. K. Wong and Y. Li, *Environ. Sci. Technol.*, 2013, **47**, 8724–8732; (f) Z. G. Yi, J. H. Ye, N. Kikugawa, T. Kako, S. X. Ouyang, H. Stuart-Williams, H. Yang, J. Y. Cao, W. J. Luo, Z. S. Li, Y. Liu and R. L. Withers, *Nat. Mater.*, 2012, **9**, 559–564.
- (a) Z. Zou, J. Ye, K. Sayama and H. Arakawa, *Nature*, 2001, **414**, 625–627; (b) K. Maeda, K. Teramura, D. Lu, T. Takata, N. Saito, Y. Inoue and K. Domen, *Nature*, 2006, **440**, 295; (c) B. C. Wang, J. Nisar, B. Pathak, T. W. Kang and R. Ahuja, *Appl. Phys. Lett.*, 2012, **100**, 182102.
- (a) K. Maeda, K. Teramura, D. Lu, N. Saito, Y. Inoue and K. Domen, *Angew. Chem., Int. Ed.*, 2006, **45**, 7806–7809; (b) K. Maeda, A. Xiong, T. Yoshinaga, T. Ikeda, N. Sakamoto, T. Hisatomi, M. Takashima, D. Lu, M. Kanehara, T. Setoyama, T. Teranishi and K. Domen, *Angew. Chem., Int. Ed.*, 2010, **49**, 4096–4099; (c) X. Zong, H. Yan, G. Wu, G. Ma, F. Wen, L. Wang and C. Li, *J. Am. Chem. Soc.*, 2008, **130**, 7176–7177; (d) J. Yang, D. Wang, H. Han and C. Li, *Acc. Chem. Res.*, 2013, **46**, 1900–1909.
- (a) H. G. Yang, C. H. Sun, S. Z. Qiao, J. Zou, G. Liu, S. C. Smith, H. M. Cheng and G. Q. Lu, *Nature*, 2008, **453**, 638–641; (b) G. Liu, J. C. Yu, G. Q. Lu and H. M. Cheng, *Chem. Commun.*, 2011, **47**, 6763–6783; (c) J. Jiang, K. Zhao, X. Y. Xiao and L. Z. Zhang, *J. Am. Chem. Soc.*, 2012, **134**, 4473–4476.
- (a) A. J. Bard, *J. Photochem.*, 1979, **10**, 59–75; (b) Q. Khaselev and J. A. Turner, *Science*, 1998, **280**, 425–427; (c) S. W. Boettcher, J. M. Spurgeon, M. C. Putnam, E. L. Warren, D. B. Turner-Evans, M. D. Kelzenberg, J. R. Maiolo, H. A. Atwater and N. S. Lewis, *Science*, 2010, **327**, 185–187; (d) A. Kay, I. Cesar and M. Grätzel, *J. Am. Chem. Soc.*, 2006, **128**, 15714–15721.
- (a) T. Kawahara, Y. Konishi, H. Tada, N. Tohge, J. Nishii and S. Ito, *Angew. Chem., Int. Ed.*, 2002, **41**, 2811–2813; (b) J. S. Zhang, M. W. Zhang, R. Q. Sun and X. C. Wang, *Angew. Chem., Int. Ed.*, 2012, **51**, 10145–10149; (c) X. Wang, Q. Xu, M. Li, S. Shen, X. Wang, Y. Wang, Z. Feng, J. Shi, H. Han and C. Li, *Angew. Chem., Int. Ed.*, 2012, **51**, 13089–13092.
- J. F. Scott, *Science*, 2007, **315**, 954–959.
- (a) J. R. White and A. J. Bard, *J. Phys. Chem.*, 1985, **89**, 1947–1954; (b) Y. Hu, X. H. Gao, L. Yu, Y. R. Wang, J. Q. Ning, S. J. Xu and X. W. Lou, *Angew. Chem., Int. Ed.*, 2013, **52**, 5636–5639.
- (a) G. Hodes, D. Cahen and J. Manassen, *Nature*, 1976, **260**, 312–313; (b) H. Reiche, W. W. Dunn and A. J. Bard, *J. Phys. Chem.*, 1979, **83**, 2248–2251.
- F. T. Wagner and G. A. Somorjai, *Nature*, 1980, **285**, 559–560.
- (a) A. Kudo and S. Hijii, *Chem. Lett.*, 1999, **10**, 1103–1104; (b) J. W. Tang, Z. G. Zou and J. H. Ye, *Catal. Lett.*, 2004, **92**, 53–56.
- H. Kato and A. Kudo, *J. Phys. Chem. B*, 2001, **105**, 4285–4292.
- (a) G. Parravano, *J. Chem. Phys.*, 1952, **20**, 342–343; (b) Y. Inoue, M. Okamura and K. Sato, *J. Phys. Chem.*, 1985, **89**, 5184–5187; (c) N. V. Burbure, P. A. Salvador and G. S. Rohrer, *Chem. Mater.*, 2010, **22**, 5823–5830; (d) A. M. Schultz, Y. L. Zhang, P. A. Salvador and G. S. Rohrer, *ACS Appl. Mater. Interfaces*, 2011, **3**, 1562–1567.
- (a) Z. G. Yi, Y. Liu, M. A. Carpenter, J. Schimer and R. L. Withers, *Dalton Trans.*, 2011, **40**, 5066–5072; (b) J. Schiemer, R. L. Withers, Y. Liu and Z. G. Yi, *J. Solid State Chem.*, 2012, **195**, 55–62; (c) G. Q. Li, Z. G. Yi, Y. Bai, W. F. Zhang and H. T. Zhang, *Dalton Trans.*, 2012, **41**, 10194–10198; (d) L. Q. Jiang, Y. Qiu and Z. G. Yi, *J. Mater. Chem. A*, 2013, **1**, 2878–2885.
- R. Von der Muhll, A. Sadel and P. Hagenmuller, *J. Solid State Chem.*, 1984, **51**, 176–182.
- T. X. Wu, G. M. Liu, J. C. Zhao, H. Hidaka and N. Serpone, *J. Phys. Chem. B*, 1998, **102**, 5845–5851.
- E. Pretsch, P. Bühlmann and C. Affolter, *Structure Determination of Organic Compounds Tables of Spectra Data*, Springer, Germany, 2002, vol. 6, pp. 255–259.
- (a) I. C. M. S. Santos, L. H. Loureiro, M. F. P. Silva and A. M. V. Cavaleiro, *Polyhedron*, 2002, **21**, 2009–2015; (b) J. F. Liu, X. L. Li and Y. D. Li, *J. Cryst. Growth*, 2003, **247**, 419–424.